Acta Geotechnica (2021) 16:1971–1981
https://doi.org/10.1007/s11440-020-01089-2

SHORT COMMUNICATION

The detailed particle breakage around the pile in coral sand

Yu Peng[1] · Hanlong Liu[2] · Chi Li[3] · Xuanming Ding[2] · Xin Deng[1] · Chunyan Wang[1]

Received: 14 March 2020 / Accepted: 12 October 2020 / Published online: 27 January 2021

Abstract
Detailed particle breakage adjacent to a pile has great influence on the settlement and bearing capacity of a pile foundation. Before the pile test, coral sand was divided into different grain-size groups and dyed in different colors, then mixed as the ground soil. After pile penetration, the sand around the pile was divided into many zones and sampled. Grains in different colors in each size range of each sample were discerned quantitatively. Results show that the settlement curve dropped fast and the skin friction of pile was small due to the obvious particle breakage. In each zone, the actual particle breakage in each size range was different from the change in relative mass percentage, and the lost of angular edges is the dominant type of particle breakage under the bottom pressure of pile. The index B_{ag}, excluding the interference effect of size overlap between fragments and unbroken grains in each size range, was slightly larger than B_g for most zones around the pile. The breakage-zone was limited to 1.5 times of the pile diameter at the radial direction and 2.5 times at the depth direction, which is much deeper than that in silica sand. Particle breakage at some distance from pile bottom is larger than that at the very bottom of the pile due to the shearing effect in the sand. Detailed particle breakage around the pile is useful in studying the interaction between the pile and crushable granular soil.

Keywords Breakage index · Breakage-zone · Detailed particle breakage · Fragments · Pile penetration

1 Introduction

The bearing capacity of the pile is mainly determined by the properties of the soil. In nature, soil is usually composed of granular materials and display crushing behavior when subjected to considerable stresses [7, 12, 21, 44, 46, 47]. With the development of civil engineering, heavier loads and crushable granular soils are frequently encountered in pile foundation engineering [4, 6, 38, 45, 48]. Particle breakage of granular materials around the pile becomes one significant aspect in studying the behavior of the pile [9, 23, 46, 51]. Particle breakage changes the contact between a pile and soil; thus the bearing capacity of the pile is decreased, and the pile displacement is obviously larger than the expected value from the conventional equations [15, 37, 41, 49, 52, 54]. Therefore, understanding particle breakage for the design and construction of pile foundations is highlighted from a practical standpoint [1, 2, 10, 37, 52, 55].

Nowadays, particle breakage is usually evaluated by particle breakage indexes related to granular size distribution (such as commonly used B_g [28], B_r [16], B_e [13], and B [14]). However, in each size range of granular

✉ Hanlong Liu
hliuhhu@163.com

Yu Peng
pengyu_lzu@163.com

Chi Li
nmglichi@imut.edu.cn

Xuanming Ding
dxmhhu@163.com

Xin Deng
csudxtunnel@163.com

Chunyan Wang
20161602084t@cqu.edu.cn

[1] College of Civil Engineering, Chongqing University, Chongqing 400450, China

[2] Key Laboratory of New Technology for Construction of Cities in Mountain Area, Chongqing University, Chongqing 400045, China

[3] Department of Civil Engineering, Inner Mongolia University of Technology, Huhhot 010051, China

materials, the broken and unbroken grains cannot be distinguished, and it is not justified in terms of better understanding the phenomenon and mechanisms. In fact, the detailed particle breakage around the pile is difficult to obtain due to the complex granular properties, the various combinations of stress, and the dispersive granular state in soil adjacent to a pile [18, 33, 42, 45]. Up to know, many scholars carried out a series of experimental test to examine the degree of particle breakage as well as its spatial distribution in the interface layers adjacent to a driven pile and showed that the particle breakage in the interface layer obviously decreased the shaft friction [1, 3, 18–20, 38, 45]. The decrease in end bearing capacity of piles in crushable materials is usually analyzed by a spherical cavity expansion theory and numerical simulations by finite element method and finite difference method [23, 37, 41, 52, 53]. However, the abovementioned methods all are from the macro-perspective. With the need for studying the microscopic mechanism of the interaction between pile and granular material, the discrete element method (DEM) has emerged [22, 23, 43]. At present, results obtained from numerical models that computes detailed crushing around piles and the interaction between detailed particle breakage and the pile have not been systematically confronted with experimental data.

Therefore, this study explores the detailed particle breakage of coral sand around the pile in the pile penetration. The dyeing, tracking, and particle image segmentation methods were introduced to distinguish the broken and unbroken grains around the pile. Then, a particle breakage index, excluded the interference effect of the broken and unbroken grains in each size range, was introduced. After that, spatial distribution characteristics of particle breakage around the pile were discussed. The methods, detailed particle breakage, and the breakage-zone around the pile are beneficial to study the settlement and bearing capacity of pile foundation in crushable granular soil.

2 Materials and methods

2.1 Sand and the dyeing

Coral sands are one of the most crushable granular soils, widely distributed in marine environments between latitudes N30° and S30° [8, 26, 39]. The coral sand in this test was obtained from the South China Sea. The natural white coral sand contains more than 94% $CaCO_3$ in weight. Following the standard ASTM D4253-14 [5], the specific gravity of the coral sand is approximately 2.78, and it is 2.65 for the silica sand used as contrasted in this test. As shown in the picture and the SEM image of Fig. 1a, the coral grains studied in this paper not only full of sharp edges but also rich in intragranular pores. To minimize the dye effect on the strength and fragmentation characteristics of sands, a neutral permeable dye agent was selected (Fig. 1b); common rocks can be penetrated by the agent about 3–8 mm. In previous laboratory one-dimensional compression test, the particle size distributions and compression curves of coral sands are very close for dyed and undyed samples during the test [34].

The relative density of the sand in this test was 65%. As shown in Fig. 1b, grains of 4 sizes: 1–2 mm, 0.5–1 mm, 0.25–0.5 mm, 0.15–0.25 mm were dyed with blue, red, green and yellow, respectively; grains with the size of 0.074–0.15 mm presented a natural white color. Then, the five size ranges of coral sands were mixed in the mass percentage as shown in Fig. 1b. To illustrate the huge effect of particle breakage on loading characteristics of pile in coral sand, one silica sand with high particle strength was contrasted in analyzing the end bearing capacity and the skin friction of piles. In this test, 7% water was added into the dry color sands to provide apparent cohesion of sands, thus preventing migration of small broken parts and ensuring the high operability of sand sample collection after the pile penetration test.

2.2 Pile penetration tests and sand sample collection

Model tests have been performed in order to better understand the bearing capacity of piles in the sandy soil. The size of the model tank is $0.8 \times 0.8 \times 1.2$ m (length $\times$ width $\times$ height). The precast pile with a diameter of 40 mm and a length of 700 mm, was cast with C32.5 concrete (cement: sand: stone: water = 1:1.11:2.72:0.38) and a reinforcement cage made with four 12# steel wires. Concrete piles were prefabricated in specific PVC tubular containers. Soil layers in the model container were filled and compacted artificially, and the relative density was checked by sampling tests. Before the penetration, scale was marked on the side of the pile by marking pen. The model test facility was comprised of a fairly rigid model container, loading system, and measuring system. A view of the model test facility is shown in Fig. 2a. The loading system consists of hydraulic jacks, loading plate, and a reaction beam. The measuring system consists of a load cell, dial gages, and a data acquisition system. During the loading tests, the load and displacement values of the pile head were measured by the load cell and dial gages, respectively. Lateral friction distribution along the pile was measured by the strain gauge pasted on the reinforcement cage. Data from the load cells and strain gauge were captured by the data acquisition system. Therefore, the end resistance of pile was acquired by the

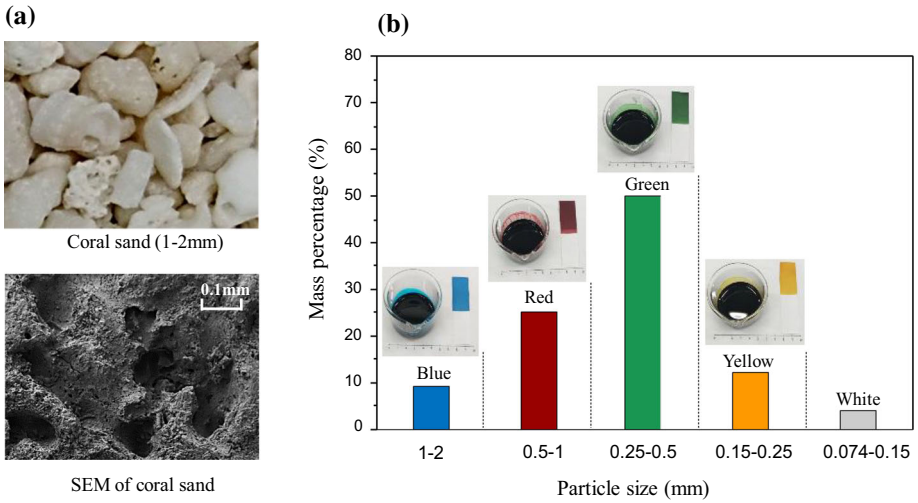

Fig. 1 **a** The coral sand, **b** dyeing agents and granular size distribution in the test

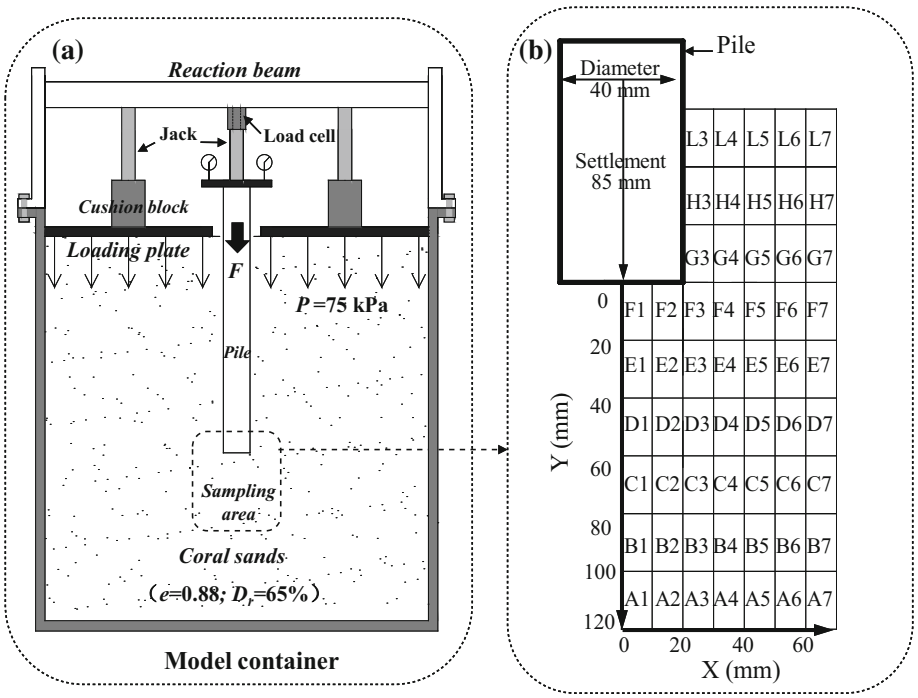

Fig. 2 Model test facilities and the sample collection: **a** the schematic diagram of pile loading, **b** the schematic of sampling areas

strain gauge near the bottom of the pile. The total skin friction of pile is inferred from the axial force (the measured strain), and it is the value of load at the pile head minus the end resistance of pile. By referring to the study of Kuwajima [19], penetration depth of the pile (diameter of 4 cm) was 85 mm and the pressure applied on the surface of the sands was 75 kPa. Same as the test of Kuwajima [19], the penetration of the model pile was displacement-controlled at 0.1 mm/min. After pile penetration, the coral sands around the pile toe were divided into many sections (Fig. 2b, A1–L7), and each sand sample in each zone around the pile was collected from the top sample layer to the bottom layer. As shown in Fig. 2b, the thickness of each sample layer is 2 cm, and the radial distance of each sample on the horizontal plane is 1 cm. The location of each section beneath the pile is determined by a rule, sticks with different lengths and strings.

2.3 Sand sample screening and particle image segmentation

After the pile penetration test and sand sample collection, soil sieves were used to separate grains in each sample into different size ranges (1–2 mm, 0.5–1 mm, 0.25–0.5 mm, 0.15–0.25 mm, 0.074–0.15 mm, < 0.074 mm). Grains that retained on the sieve that initially retained them before the test are termed as "residual grains". In contrast, grains that passed the sieve that initially retained them are termed as "fragments" [35]. For example, a blue grain in 1–2 mm sieve could be labeled "residual grain", a blue fragment with size of 0.5–1 mm passing through one sieve could be labeled "1st tier fragment", and a blue fragment with size of 0.25–0.5 mm passing through two sieves could be labeled "2nd tier fragment" (Fig. 3a).

To distinguish the broken and unbroken grains in each size range, the grains in each sieve were homogeneously poured into different round dishes (diameter of 10 cm) and photographed with a high-resolution digital camera. As shown in Fig. 3b, the internal color of particles is light, but it is not difficult to discerning the particle due to the follow reasons: (1) before the grain discerning process, grains in different size range is separated by sieves; (2) during the color threshold process in the software Image J, parameters can be adjusted to well including the internal light color as shown in Fig. 3b. The partial enlarged figure of particle discerning in each size range as shown in Fig. 3c, and the detailed process can refer to the previous studies [3, 11, 32, 35, 54, 55]. (3) Three images of coral sand in each round dish were used to find the average area ratio of color grains in one size range (mixing the sand homogenously before taking each photograph). Grains with different colors in each size range are discerned, respectively, by repeating similar operation shown in Fig. 3 for each image.

The area percentage of each kind of color grains in an image is close to the mass percentage of the kind of color grains due to the similar grain size in a sieve. The relationship between mass and area in a size range (a sieve) can be given as follows:

$$\frac{S_{\mathrm{i}}}{S_{\mathrm{all}}} \approx \frac{\pi r^2 n_{\mathrm{i}}}{\pi r^2 n_{\mathrm{all}}} \approx \frac{n_{\mathrm{i}}}{n_{\mathrm{all}}}$$

$$\frac{m_{\mathrm{i}}}{m_{\mathrm{all}}} = \frac{\rho V_{\mathrm{i}}}{\rho V_{\mathrm{all}}} \approx \frac{\rho \cdot \frac{3}{4}\pi r^3 n_{\mathrm{i}}}{\rho \cdot \frac{3}{4}\pi r^3 n_{\mathrm{all}}} \approx \frac{n_{\mathrm{i}}}{n_{\mathrm{all}}}$$

$$\frac{m_{\mathrm{i}}}{m_{\mathrm{all}}} \approx \frac{S_{\mathrm{i}}}{S_{\mathrm{all}}} \tag{3}$$

where S_{i} is the area covered by a certain color grains in the selected image (i.e., one of the areas with the blue, red, green, yellow, and white color in the image); S_{all} is the total area covered by all color grains for the selected image; r is the mean radius of grains in the selected image; n_{i} is the numbers of a certain color grains; n_{all} is the total numbers of all grains; m_{i} is the mass of a certain color grains in the selected image (i.e., one of the mass of blue, red, green, yellow, and white grains in the size range); m_{all} is the total mass of grains in the selected image; ρ is the grain density; V_{i} is the volume of a certain color grains; V_{all} is the total volume of all color grains in the selected image.

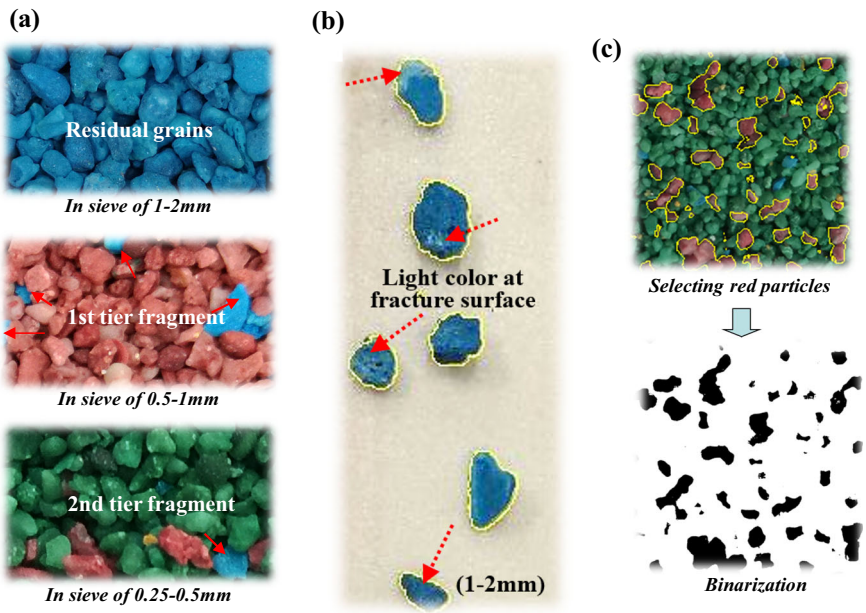

Fig. 3 **a** Residual grains and fragments after sieving, **b** discerning the fracture surface of blue grains, **c** grain discerning process

3 Results and discussions

3.1 End bearing capacity and the total skin friction of pile

End bearing capacity and total skin friction values plotted against normalized settlement *S*/*D* (where *S* is pile settlement (penetration depth) and *D* is pile diameter) are shown in Fig. 4. The normalized settlement of the pile in the coral sand presented a steep drop compared with that in the silica sand as shown in Fig. 4a. Figure 4b shows that the peak skin friction occurred at a displacement of about *S*/*D* = 0.1, which is similar to the study of Kuwajima [19]. Further displacement caused a rapid decrease in skin friction for piles in both sands, and the decrease in skin friction in coral sand was much more drastic than that in silica sand. The normal stress on pile sides decreased due to the volume shrinkage of soil after particle breakage, which decreased the skin friction on the pile [1, 19, 38]. Different from the pile in silica sand, during the pile penetration test in coral sand, the sudden drop in stress was observed in the data acquisition system and even the sound of particle breakage was heard. Therefore, considering particle breakage around the pile in coral sand was especially significant.

3.2 Detailed particle breakages in each size range of one zone

When considering the particle breakage, one of the latest breakthroughs of the mathematical model is the Markov Chain Model as shown in Fig. 5a [40]. The model reveals the detailed particle behavior during the whole process of particle breakage, and the survival probability ($S_{i,i}$) and the probability of particle breakage ($P_{i,i}$) is given in the model [36]. However, corresponding experimental methods are lacking to get the $S_{i,i}$ and $P_{i,i}$. The $S_{i,i}$ and $P_{i,i}$ can be

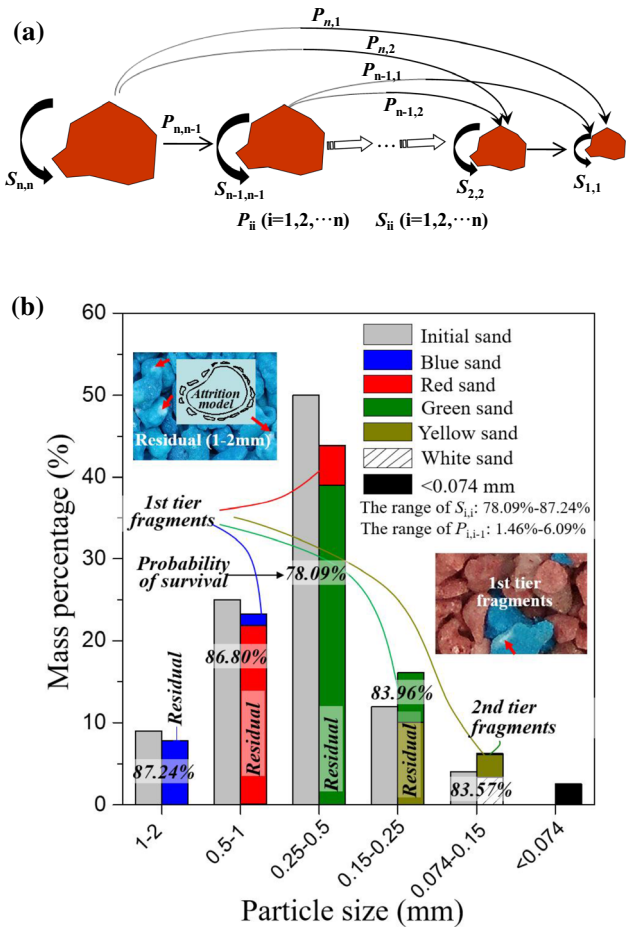

Fig. 5 **a** The detailed probability of particle breakage (P_{ii}) and survival (S_{ii}) for grains (Tong et al. [40]), **b** detailed granular size distribution of sand under the bottom of pile (Section E1)

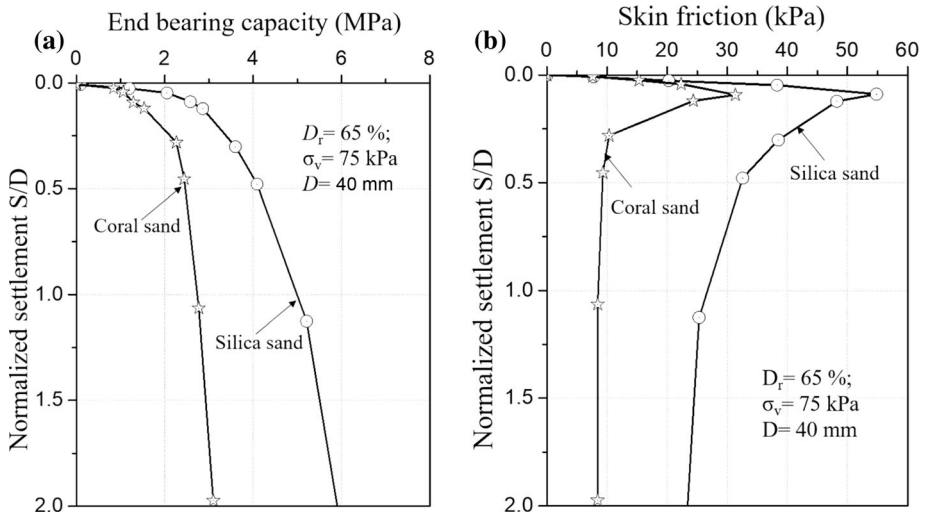

Fig. 4 **a** End bearing capacity versus normalized settlement, **b** skin friction versus normalized settlement

obtained by the detailed particle breakage (mass percentage of residual grains and fragments) in this test.

Detailed particle breakage of coral sand under bottom of the model pile (taking the E1 zone in Fig. 2b as an example) is shown in Fig. 5b. The detailed probability of particle survival in each size range and the detailed mass percentage of fragments are shown in Fig. 5b. The commonly used index to evaluate the particle breakage in each size range is the relative particle breakage which is the value of mass percentage of initial grains minus the mass percentage of grains in the same size range after particle breakage. Figure 5b shows that the actual amount of particle breakage in size range of 0.25–1 mm is obviously larger than the amount of relative particle breakage, while particle breakage in the size range of 0.074–0.25 mm is slightly smaller than the amount of relative particle breakage. The actual amount of particle breakage in each size range should be the initial mass percentage minus the mass percentage of residual grains in the size range. Therefore, relative particle breakage is different from the actual amount of particle breakage in each size range.

Besides, vast majority of fragments presented in the 1st smaller size range while the amount of the 2nd tier fragments is very small (Fig. 5b, also can see images in Fig. 3a); the range of $S_{i,i}$ is 78.09%–87.24% while the range of $P_{i,i-1}$ is 1.46%–6.09%. Therefore, the lost of angular edges of grains (the attrition model, as shown in images of Fig. 5b) is the dominant type of breakage under the bottom pressure of pile. Very few coral grains are crushed with fracture model (a grain splitting into several smaller grains of similar sizes) though the coral sand is rich in intragranular pores.

3.3 The amount of particle breakage for each zone around the pile

Detailed particle breakage of each zone around the pile can be obtained using the dyeing, tracking, and particle image segmentation methods. However, it was still difficult to evaluate the actual amount of particle breakage in each zone around the pile, excluding the interference effect of size overlaps between broken and unbroken grains. This part gives a quantitative particle breakage index of sand samples for each zone.

One of the commonly used particle breakage indexes is the B_g proposed by Marsal [28]. The B_g can be calculated using:

$$B_g = \sum_{i=1}^{n} |a_i - b_i| = |a_1 - b_1| + |a_2 - b_2| + \cdots + |a_n - b_n| \tag{4}$$

where a_i and b_i is the mass percentage of particles in the size range i before and after particle breakage, respectively, and the value of $(a_i - b_i)$ can be positive or negative; n is the total number of size ranges for a particle sample; $\sum$ stands for adding up the mass percentage from the largest particle to the smallest one.

By analogy with the definition of current grading in Fig. 6a, the residual grading of a particle sample was defined as adding up the mass percentage of residual grains in total particles from the smallest grain to the largest one. The breakage index B_{ag}, excluding the interference effect of the coexistence of broken and unbroken grains in each size, can be expressed as:

$$B_{ag} = \sum_{i=1}^{n} |c_i - d_i| = |c_1 - d_1| + |c_2 - d_2| + \cdots + |c_n - d_n| \tag{5}$$

where c_i is the mass percentage of particles in the size range i before particle breakage in Fig. 6a; d_i is the mass percentage of residual particles in size range i after particle

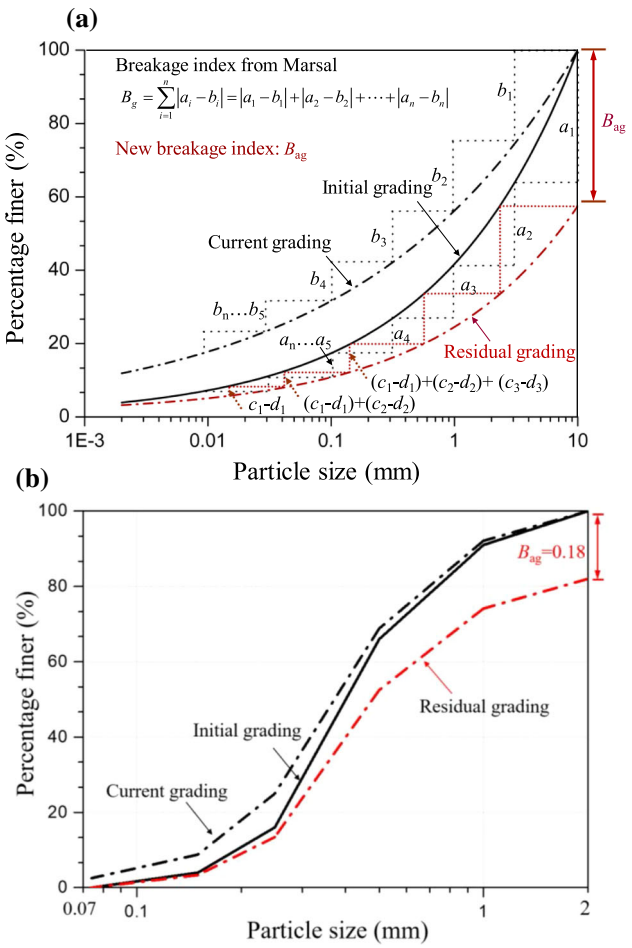

Fig. 6 **a** The definition of particle breakage indexes B_g and B_{ag}, **b** the calculation of particle breakage B_{ag} for the zone E1

breakage; $\sum$ stands for adding up the mass percentage from the smallest particle to the largest one.

According to Eq. 5, the value of $(c_i - d_i)$ is positive constantly, and the vertical height between the top of the initial grading and the residual grading happens to be B_{ag} (Fig. 6a). Therefore, different from B_g, the theoretical value of B_{ag} is 0–1, and is simple for calculation. With the use of B_{ag}, a clear relationship between probability of grain survival S_i in each size range (directly connect to the Markov Chain Model) and the actual amount of particle breakage of particle samples was established from the process-based perspective. Moreover, detailed probabilities of grain survival and the index B_{ag}, excluding the interference effect of the coexistence of fragments and unbroken grains, have a more specific and clear physical meaning, facilitating the understanding of the phenomenon and mechanisms involved. As an example, Fig. 6b shows the residual grading and current grading for sand in the zone E1 (at the bottom of the pile). It can be easily observed that the breakage index B_{ag} of sand sample in the zone E1 is 0.18.

In the previous study, most relevant researches are the breakage-result-based study. The particle breakage effect on soil behavior is base on the final results of particle breakage (contrasting the PSD before and after the test), and the result between pressure (P) and void ratio (e) is further used in computing and simulating the behavior of the pile foundation in granular material [2, 19, 24, 29, 46]. However, with the need for studying the microscopic mechanism of soil behavior induced by structures, detailed process-based research has emerged [5, 23, 40]. Detailed fragments and the detailed probability of particle breakage are relevant to the models of particle breakage (fracture, attrition, and abrasion) and the energy dissipation around the pile [40, 41, 48]. At present, the interaction between pile and granular material could be simulated from in a micro-process-based way by using the discrete element method (DEM) [22, 43]; therefore, the detailed fragments and probability of particle breakage in this study can be used to verify the results in simulations. The index B_{ag} realized the unification from each particle size to the whole sample from the detailed micro-process-based perspective, and makes it is possible to compare with previous commonly used index from breakage-result-based studies.

3.4 Evaluation of particle breakage around the pile

As a contrast, the particle breakage of the common silica sand is very small, the value of B_g is about 0.04 at the bottom of pile (the E1 section, see Fig. 2b); therefore, it is difficult to measure the distribution of particle breakage around the pile under the top pressure of 75 kPa in silica sand. However, the particle breakage of coral sand around the pile was large under the top pressure of 75 kPa. The B_g and B_{ag} values of coral sand for each zone are plotted against the normalized vertical distance from the base of the pile Y/D and the radial distance from the center of the pile X/D in Fig. 7a, b. The value of B_{ag} is only slightly larger than the value of B_g in most zones around the pile in Fig. 7, which is consistent with the aforementioned phenomenon that actual amount of particle breakage in large size ranges is larger than the amount of relative particle breakage while it is slightly smaller in small size ranges. The B_{ag} obtained from the detailed particle breakage has a value similar to B_g, which means that the index B_{ag} is appropriate in application. As to the distribution of particle breakage around the pile, the B_g and B_{ag} values became larger as decrease the distance from the base of pile in Fig. 7a, b (exception the section of F1, close to the base of pile). The distribution consistent with common sense that the closer to the pile, the higher extent of particle breakage. The progressive line in Fig. 7a, b corresponds to the value of 0.05, which indicates the boundary of breakage-zone, and the breakage is caused by the pressure process on the sand surface and the screening of sand. The stationary points of curves in Fig. 7a indicated that the obvious particle breakage was limited to 2.5 times of the pile diameter at the depth direction, while it was limited to 1.0 times of the pile diameter at the radial direction as shown in Fig. 7b. The obvious particle breakage zone in this test is close to the results in Kuwajima's study [19] (Fig. 8a), which was conducted in the Chiibishi sand ($CaCO_3$ content of 96%).

However, as shown in Fig. 8b, the obvious particle breakage zone in silica sand is only about 1.0 times of the pile diameter to the flat base of pile (upper of the pile tip) at depth direction in the previous studies [50, 52, 53]. The deeper breakage-zone in this test and Kuwajima's study should be owing to the obvious particle breakage of coral sand, which decreased the lateral restraint and further lead to the concentration of stress in the depth direction. The deeper breakage-influenced zone in coral sand can also be explained by the modulus ratio of double foundation. Because the modulus of sandy soil is proportional to the relative density of sand [17, 25, 31], the penetration of pile increased the modulus of sandy soil close to the pile tip. Compared with silica sand, obvious particle breakage of coral sand decreased the increment of modulus under same penetration depth (compression volume). Therefore, the modulus ratio of upper soil to lower soil in coral sand is smaller than that in silica sand, and the pressure is concentrated in the direction of depth.

Different from Kuwajima's study, the amount of particle breakage close to the bottom of pile is not largest. Therefore, a simple discrete element model method was used to qualitatively verify the results in this test as shown in

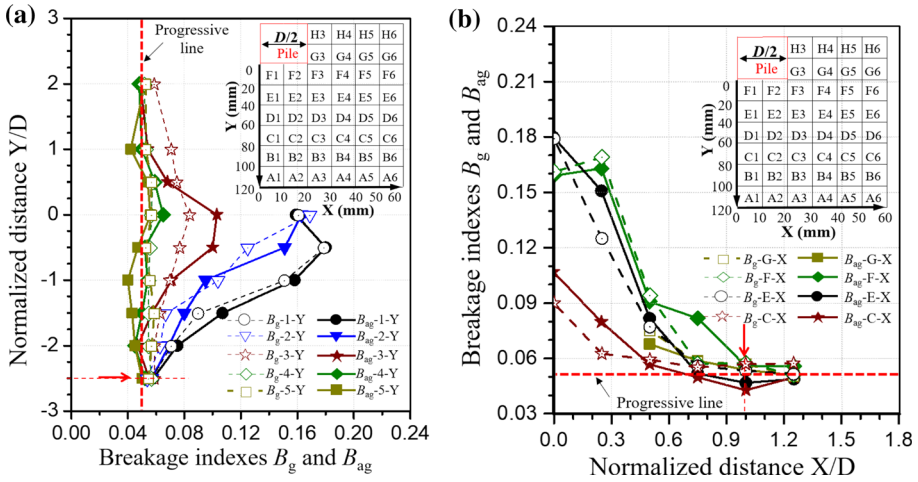

Fig. 7 Particle breakage around the pile: **a** breakage indexes B_g and B_{ag} relative to base of pile, **b** breakage indexes B_g and B_{ag} relative to radial distance from center of pile

Fig. 8c, coral grains are simulated by fragmentable clusters, and the position of lost bands are displayed with red markers. Each cluster is composed of several balls bonded by the linear contact bond model. The size range of clusters is 1–3 mm, and bonding gap between balls in each cluster is 0. The friction between each cluster is 0.5. The size of the pile and pressure on the surface of soil in the numerical simulation is same as the experimental test in this study. Result in Fig. 8c is consistent with the result in experiment study that particle breakage at some distance from pile bottom is larger than that at the very bottom of the pile, which can be explained by the classic compression zone and the shearing areas under the bottom of pile according to the Meyerhof's study [30]. For displacement piles, the process of pile penetration can be considered as soil streams passing through a stationary pile [45]. A shear band is well formed after continuous pile penetration with the soil's flow over the pile shaft. Compared with sand in the compression zone, the sand in the shearing areas is much easier for rotation and movement, which lead to the angular edge loss of grains. The un-observed compression zone effect on the amount of particle breakage in Kuwajima's results should be attributed to the smaller pile diameter of 3 cm and the sampling process that sands in the small compression zone and shearing zone had been divided into one sampling area.

As described above, a schematic illustration of particle breakage distribution around the end of pile tip is acquired in Fig. 8d. The particle breakage in the shear zone is larger than that in the compression zone and other zones. Since shear failure is the most typical form of pile foundation failure, it is necessary to pay more attention to particle breakage within the shear zone. Besides, the breakage-influenced depth in coral sand can be up to 2.5 times of the pile diameter. Except for the fast decreased in lateral friction of pile, the deep breakage-influenced zone under pile end should also be a reason for the fast drop of pile in coral sand during the loading and penetration processes. Moreover, the obvious largest breakage in the shear zone and the deeper breakage-influenced depth in coral sand may induce the underestimating the extent of particle breakage and settlement of pile in studies as mentioned previously, which may eventually overestimate the ground bearing capacity.

4 Conclusions

By applying the dyeing, tracking, and particle image segmentation method to coral sand that was used in the pile penetration test, the detailed particle breakage around the pile was investigated. The main conclusions are as follows:

(1) Compared with pile in silica sand, the end bearing of pile in coral sand presented a steeper drop as the increase in displacement, and the skin fraction of pile in coral sand dropped much faster after the peak skin friction due to the obvious particle breakage of coral sand.

(2) The detailed amount of various-sized fragments and residual grains in each zones around the pile can be obtained, and actual particle breakage in each size range is different from the relative mass percentage due to the coexistence of broken and unbroken grains. The lost of angular edges is the dominant type of particle breakage for coral sand under the bottom pressure of pile.

(3) The index B_{ag}, excluding the interference effect of size overlap between broken and unbroken grains in each size range, was proposed to evaluate the actual

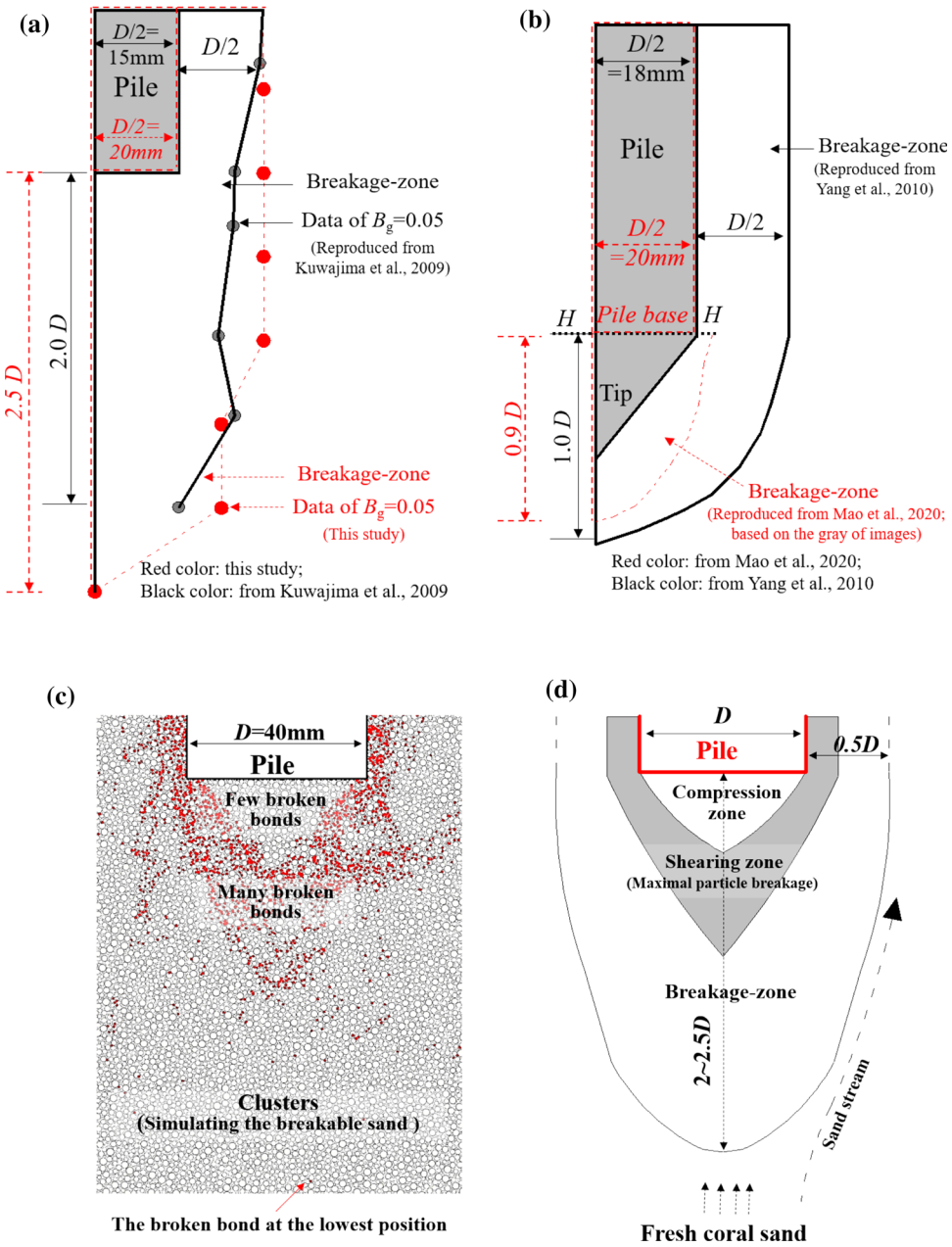

Fig. 8 The breakage-zone around the pile end during the pile penetration: **a** penetration in coral sand, **b** penetration in silica sand (Reproduced from Yang et al. [50] and Mao et al. [27]), **c** penetration simulation by discrete element software, **d** the sketch map of breakage zone in coral sand

particle breakage around the pile. Different from breakage index B_g, the theoretical value of B_{ag} is 0–1, and is simple for calculation. Besides, the index B_{ag} is a little larger than B_g for most zones around the pile.

(4) The obvious particle breakage in the coral sand is limited to 1.5 times of the pile diameter at the radial direction and about 2.5 times of the pile diameter at the depth direction, which is much deeper than that in silica sand. The particle breakage at some distance from pile bottom is larger than the particle breakage at the very bottom of piles, which can be explained as the compression zone and the shearing zone under piles.

Since detailed breakage around a pile is dependent on the state of particle and energy dissipation from new surface fracture, attrition, abrasion, etc., the detailed breakage and the index could promote the understanding the detailed behavior during the pile-soil interaction. The breakage-zone around the end of a pile is beneficial to study the

settlement and bearing capacity of pile foundation in crushable granular soil.

Acknowledgements This work was supported by the National Natural Science Foundation of China with Grant Number 51878103 and 41831282; Fundamental Research Funds for the Central Universities with Grant ID 2019CDJDTM0007).

Compliance with ethical standards

Conflict of interest The authors declare that they have no conflict of interest.

References

1. Alba JL, Audibert JME (1999) Pile design in calcareous and carbonaceous granular materials. In: Proceedings of 2nd international conference on engineering for calcareous sediments, Bahrain, pp 29–43
2. Altuhafi F, Jardine RJ (2011) Effect of particle breakage and strain path reversal on the properties of sands located near to driven piles. In: Proceedings of 5th international symposium on deformation characteristics of geomaterials, Seoul, pp 388–395.
3. Altuhafi F, O'Sullivan C, Cavarretta I (2013) Analysis of an image-based method to quantify the size and shape of sand particles. J Geotech Geoenviron 139(8):1290–1307. https://doi.org/10.1061/(ASCE)GT.1943-5606.0000855
4. Altuhafi F, Jardine RJ, Georgiannou VN, Moinet W (2018) Effects of particle breakage and stress reversal on the behaviour of sand around displacement piles. Geotechnique 68(6):546–555
5. ASTM D (1994) Standard test method for specific gravity of soil solids by gas pycnometer. Annu Book standards 4:376–379
6. Cao GW, Chen ZX, Wang CL, Ding XM (2020) Dynamic responses of offshore wind turbine considering soil nonlinearity and wind-wave load combinations. Ocean Eng 63:19–35.
7. Casini F, Viggiani GM, Springman SM (2013) Breakage of an artificial crushable material under loading. Granul Matter 15(5):661–673
8. Coop MR, Sorensen KK, FreitasT B, Georgoutsos G (2004) Particle breakage during shearing of a carbonate sand. Geotechnique 54(3):157–163
9. Daouadji A, Hicher PY (2010) An enhanced constitutive model for crushable granular materials. Int J Numer Anal Methods Geomech 34(6):555–580
10. Datta M, Gulhati SK, Rao GV (1979) Crushing of calcareous sands during shear. In: Proceedings of 11th ann. offshore technol. conf., Houston, TX, pp 1459–1467
11. De AJC, Wang XZ, Roberts KJ (2005) Multi–scale segmentation image analysis for the in–process monitoring of particle shape with batch crystallisers. Chem Eng Sci 60(4):1053–1065
12. Ding XM, Zhang YL, Wu Q, Chen ZX, Wang CL (2021). Shaking table tests on the seismic responses of underground structures in coral sand. Tunn Undergr Sp Tech, 109:103775
13. Einav I (2007a) Breakage mechanics—part I: theory. J Mech Phys Solids 55(6):1274–1297
14. Einav I (2007b) Fracture propagation in brittle granular matter. Proc R Soc A Math Phys Eng Sci 463(2087):3021–3035
15. Golightly CR, Hyde AFL (1988) Some fundamental properties of carbonate sands. In: Proceedings of the international conference on calcareous sediments, Perth, Australia, vol 1, pp 69–78
16. Hardin BO (1985) Crushing of soil particles. J Geotech Eng 111(10):1177–1192
17. Håkansson I, Lipiec J (2000) A review of the usefulness of relative bulk density values in studies of soil structure and compaction. Soil Tillage Res 53(2):71–85
18. Jin YF, Yin ZY, Wu ZX, Zhou WH (2018) Identifying parameters of easily crushable sand and application to offshore pile driving. Ocean Eng 154:416–429
19. Kuwajima K, Hyodo M, Hyde AF (2009) Pile bearing capacity factors and soil crushability. J Geotech Geoenviron Eng 135(7):901–913
20. Liu BL, Yang H, Karekal S (2020) Effect of water content on argillization of mudstone during the tunnelling process. Rock Mech Rock Eng 53(2):799–813
21. Liu F, Yi J, Cheng P, Yao K (2020) Numerical simulation of setup around shaft of XCC pile in clay. Geomech Eng 21(5):489–501
22. Liu S, Wang J (2016) Depth-independent cone penetration mechanism by a discrete element method (DEM)-based stress normalization approach. Can Geotech J 53(5):871–883
23. Lobo-Guerrero S, Vallejo LE (2007) Influence of pile shape and pile interaction on the crushable behavior of granular materials around driven piles: DEM analyses. Granul Matter 9(3–4):241
24. Luan L, Ding X, Zheng C, Kouretzis GP, Wu Q (2019) Dynamic response of pile groups subjected to horizontal loads. Can Geotech J. https://doi.org/10.1139/cgj-2019-0031
25. Luan L, Zheng C, Kouretzis GP, Ding X (2020) Dynamic analysis of pile groups subjected to horizontal loads considering coupled pile-to-pile interaction. Comput Geotech 2020:117. https://doi.org/10.1016/j.compgeo.2019.103276
26. Ma, GL, He X, Jiang X, Liu HL, Xiao Y (2020) Strength and permeability of bentonite-assisted biocemented coarse sand. Can Geotech J. https://doi.org/10.1139/cgj-2020-0045
27. Mao WW, Hamaguchi H, Koseki J (2020) Discrimination of particle breakage below pile tip after model pile penetration in sand using image analysis. Int J Geomech 20(1):04019142
28. Marsal RJ (1967) Large-scale testing of rockfill materials. J Soil Mech Found Div 93(2):27–43
29. Meng K, Cui CY, Li HJ (2020) An ontology framework for pile integrity evaluation based on analytical methodology. IEEE Access 8(99):1
30. Meyerhof GG (1951) The ultimate bearing capacity of foudations. Geotechnique 2(4):301–332
31. Mohammadi SD, Nikoudel MR, Rahimi H, Khamehchiyan M (2008) Application of the Dynamic Cone Penetrometer (DCP) for determination of the engineering parameters of sandy soils. Eng Geol 101(3–4):195–203
32. Ohm HS, Hryciw RD (2013) Translucent segregation table test for sand and gravel particle size distribution. Geotech Test J 36(4):592–605
33. Ovalle C, Dano C, Hicher PY, Cisternas M (2015) Experimental framework for evaluating the mechanical behavior of dry and wet crushable granular materials based on the particle breakage ratio. Can Geotech J 52(5):587–598
34. Peng Y, Ding X, Xiao Y, Chu J, Deng W (2019) Study of particle breakage behaviour of calcareous sand by dyeing tracking and particle image segmentation method. Rock Soil Mech 40(7):2663–2672
35. Peng Y, Ding X, Xiao Y, Deng X, Deng W (2020) Detailed amount of particle breakage in non-uniformly graded sands under one-dimensional compression. Can Geotech J 57:1239–1246
36. Peng Y, Ding XM, Zhang Y, Wang CL, Wang CY (2021) Evaluation of the particle breakage of calcareous sand based on the detailed probability of grain survival: an application of repeated low-energy impacts. Soil Dyn Earthq Eng 141:106497
37. Poulos HG, Chua EW (1985) Bearing capacity of foundations on calcareous sand. In: Proceedings of 11th international conference

on soil mechanics and foundation engineering, San Francisco, CA, vol 3, pp 1619–1622
38. Tanaka K, Yasufuku N, Murata H, Hiyodo M (1995) Engineering properties of carbonate sands and skin friction of pile in sands. Doboku Gakkai Ronbunshu 1995(523):99–109
39. Tong CX, Burton GJ, Zhang S, Sheng D (2020) Particle breakage of uniformly graded carbonate sands in dry/wet condition subjected to compression/shear tests. Acta Geotech. https://doi.org/10.1007/s11440-020-00931-x
40. Tong CX, Zhang KF, Zhang S, Sheng D (2019) A stochastic particle breakage model for granular soils subjected to one-dimensional compression with emphasis on the evolution of coordination number. Comput Geotech 112:72–80
41. Tovar-Valencia RD, Galvis-Castro A, Salgado R, Prezzi M (2017) Effect of surface roughness on the shaft resistance of displacement model piles in sand. J Geotech Geoenviron Eng 144(3):04017120
42. Tsoungui O, Vallet D, Charmet JC (1999) Numerical model of crushing of grains inside two-dimensional granular materials. Powder Technol 105(1–3):190–198
43. Wang J, Zhao B (2014) Discrete-continuum analysis of monotonic pile penetration in crushable sands. Can Geotech J 51(10):1095–1110
44. Wang Z, Li C, D X, (2019) Application of transparent soil model tests to study the soil-rock interfacial sliding mechanism. J Mt Sci 16(4):935–943
45. White DJ, Bolton MD (2004) Displacement and strain paths during plane-strain model pile installation in sand. Geotechnique 54(6):375–397
46. Wu Y, Yamamoto H, Yao Y (2013) Numerical study on bearing behavior of pile considering sand particle crushing. Geomech Eng 5(3):241–261
47. Xiao Y, Liu H, Chen H, Stuedlein AW, Evans TM, Chu J, Liang Cheng, Jiang NJ, Lin H, Liu HL, Aboel-Naga HM (2020) Restraint of particle breakage by biotreatment method. J Geotech Geoenviron Eng 146(11):04020123
48. Xiao Y, Yuan Z, Chu J, Liu H, Huang J, Luo SN, Lin J (2019) Particle breakage and energy dissipation of carbonate sands under quasi-static and dynamic compression. Acta Geotech 14(6):1741–1755
49. Yamamoto N, Randolph MF, Einav I (2009) A numerical study of the effect of foundation size for a wide range of sands. J Geotech Geoenviron Eng 135(1):37–45
50. Yang ZX, Jardine RJ, Zhu BT, Foray P, Tsuha CHC (2010) Sand grain crushing and interface shearing during displacement pile installation in sand. Geotechnique 60(6):469–482
51. Yasufuku N, Ochiai H, Ohno S (2001) Pile end-bearing capacity of sand related to soil compressibility. Soils Found 41(4):59–71
52. Zhang C, Einav I, Nguyen GD (2013) The end-bearing capacity of piles penetrating into crushable soils. Geotechnique 63(5):341–354
53. Zhang C, Yang ZX, Nguyen GD, Jardine RJ, Einav I (2014) Theoretical breakage mechanics and experimental assessment of stresses surrounding piles penetrating into dense silica sand. Geotech Lett 4(1):11–16
54. Zheng WB, Hu XL, Tannant DD (2020) Shape characterization of fragmented sand grains via x-ray computed tomography imaging. Int J Geomech 20(3):04020003.1-04020003.14
55. Zheng WB, Hu XL, Tannant DD, Zhang K, Xu C (2019) Characterization of two-and three-dimensional morphological properties of fragmented sand grains. Eng Geol 263(20):105358